Supporting Information

Ligand-Dependent Assembly of Dinuclear, Linear Tetranuclear and One-dimensional Zn(II) Complexes with Aroylhydrazone Schiff base

Guohong Xu,[a] Gu-ilei Liu,[b] Bei-bei Tang[a] and Hui Li *[a]

[a] *Key Laboratory of Cluster Science of Ministry of Education, School of Chemistry and Chemical Engineering, Beijing Institute of Technology, Beijing 100081, P. R. China.*

**E-mail address: lihui@bit.edu.cn; Tel: 86-10-68912667*

[b] *National Research Center for Geoanalysis*

Contents

Section 1 Synthesis of the H_3L^1, H_4L^2, H_2L^3

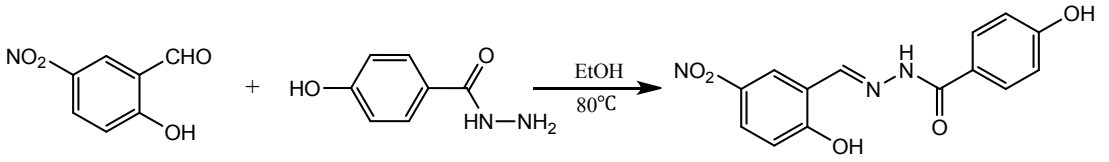

5-Nitrosalicylaldehyde

4-Hydroxybenzhydrazide

4-Hydroxy-benzoic acid (2-hydroxy-5-nitro-benzylidene)-hydrazide

Scheme S1 Synthetic route of the ligand H_3L^1.

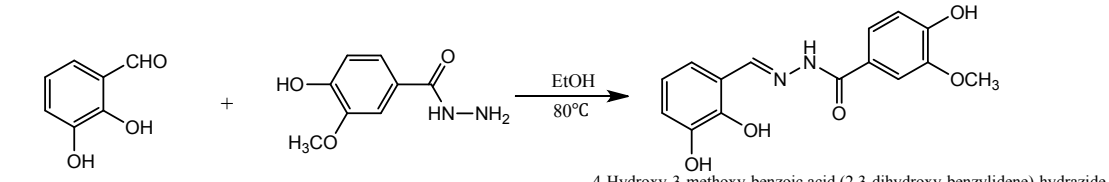

2,3-Dihydroxy-benzaldehyde

4-Hydroxy-3-methoxy-benzoic acid hydrazide

4-Hydroxy-3-methoxy-benzoic acid (2,3-dihydroxy-benzylidene)-hydrazide

Scheme S2 Synthetic route of the ligand H_4L^2.

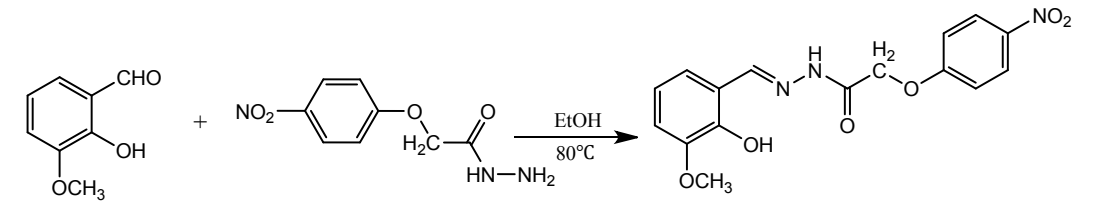

2-Hydroxy-3-methoxy-benzaldehyde

(4-Nitro-phenoxy)-acetic acid hydrazide

(4-Nitro-phenoxy)-acetic acid (2-hydroxy-3-methoxy-benzylidene)-hydrazide

Scheme S3 Synthetic route of the ligand H_2L^3.

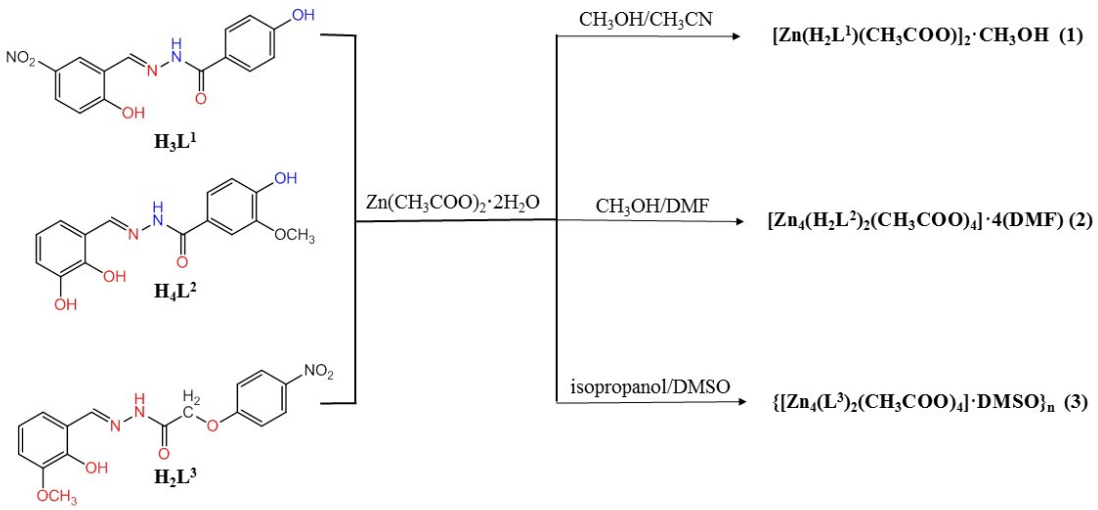

Scheme S4 The reaction representations of the complexes **1-3**.

Section 2 ^{1}H NMR and ^{13}C NMR spectra of the H_3L^1, H_4L^2, H_2L^3

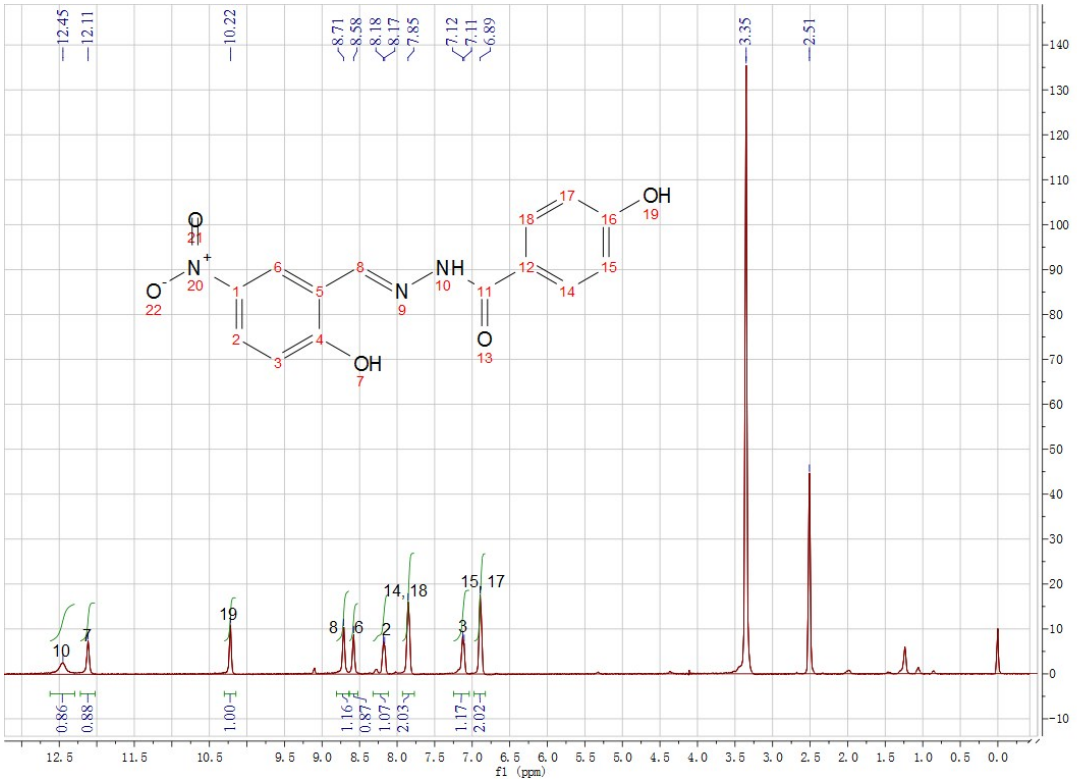

Fig. S1 ^{1}H NMR spectra of the ligand $\mathbf{H_3L^1}$ in DMSO-d^6 solution.

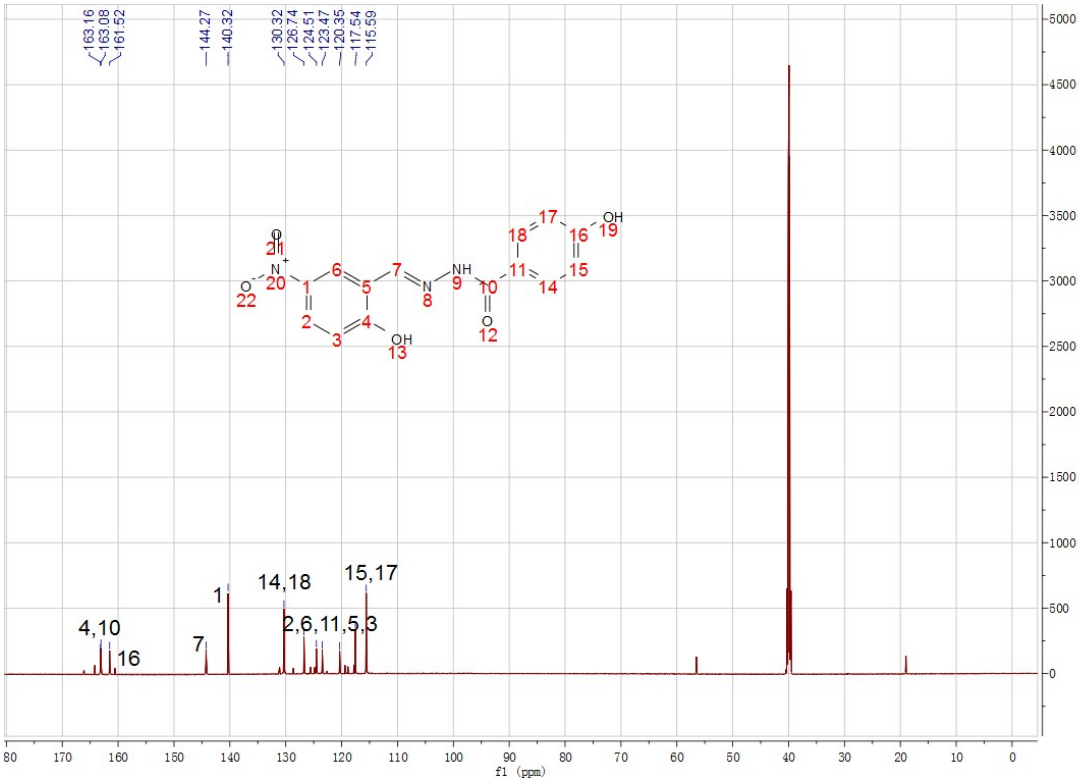

Fig S2. ^{13}C NMR spectra of the ligand $\mathbf{H_3L^1}$ in DMSO-d^6 solution.

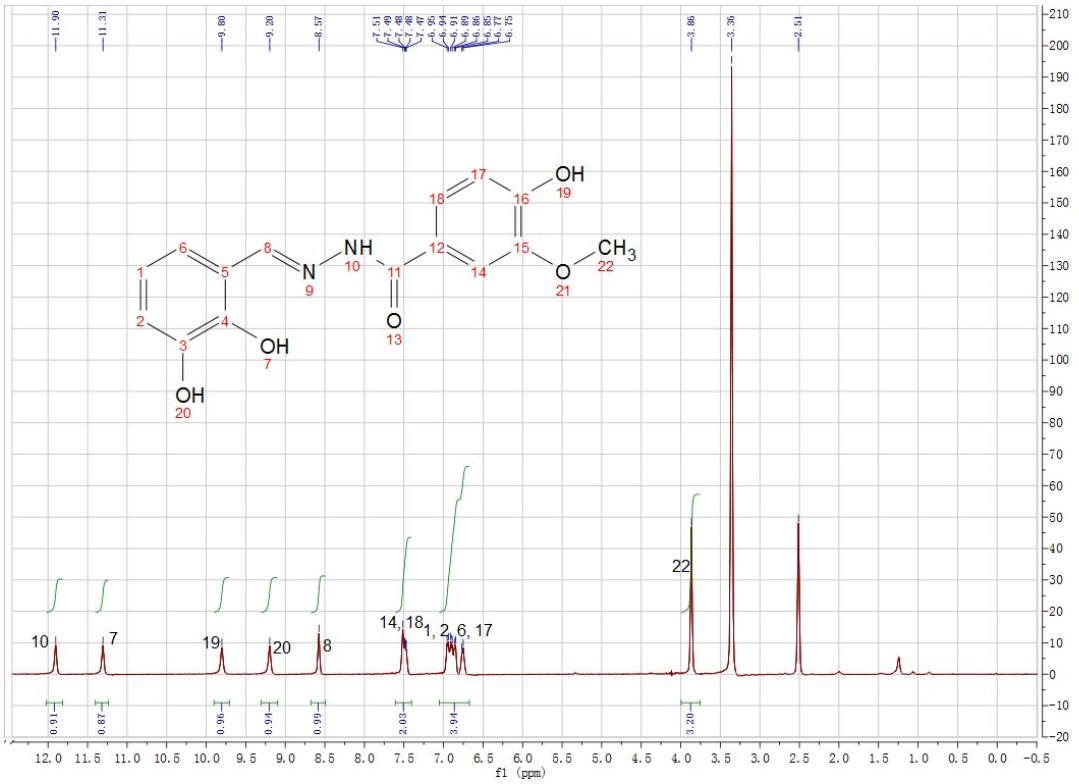

Fig. S3 ^{1}H NMR spectra of the ligand $\mathbf{H_4L^2}$ in DMSO-d^6 solution.

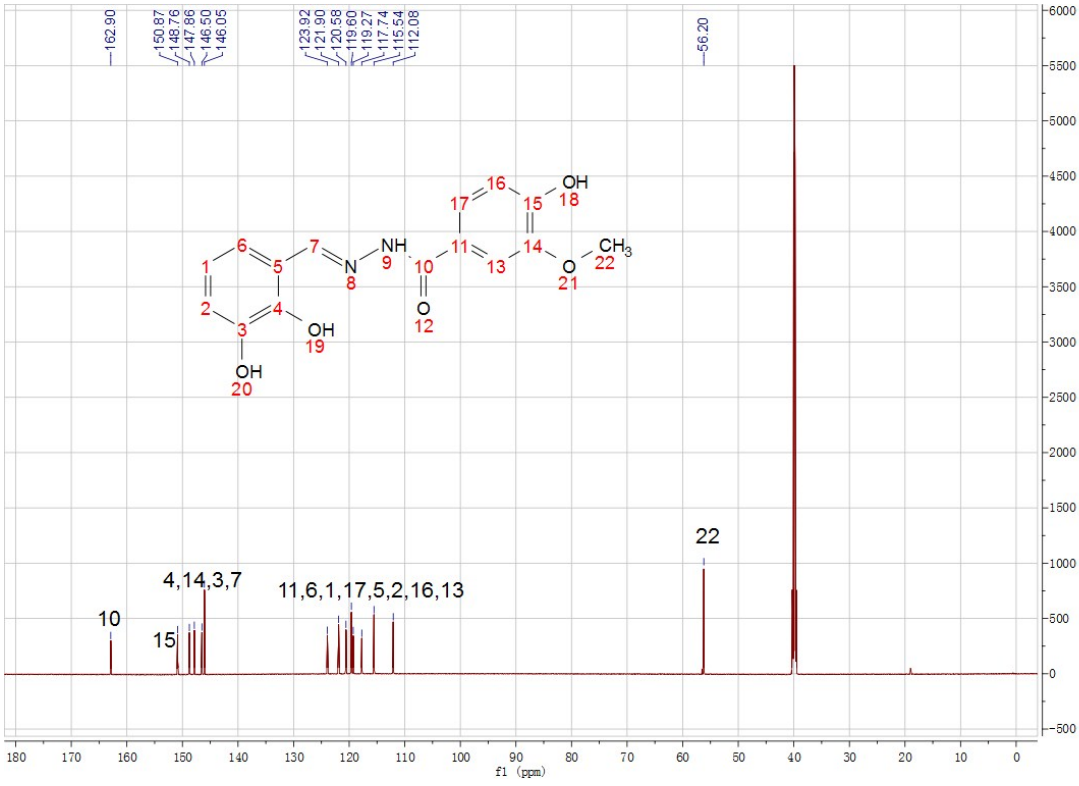

Fig. S4 ^{13}C NMR spectra of the ligand $\mathbf{H_4L^2}$ in DMSO-d^6 solution.

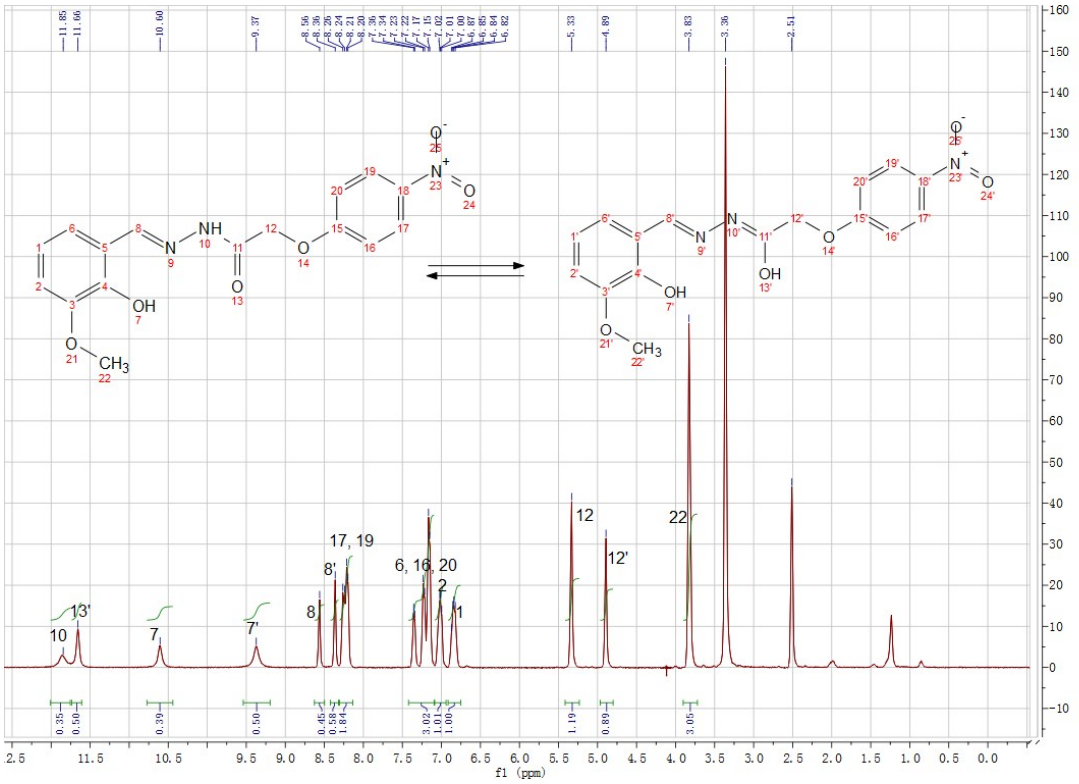

Fig. S5 ^{1}H NMR spectra of the ligand $\mathbf{H_2L^3}$ in DMSO-d^6 solution.

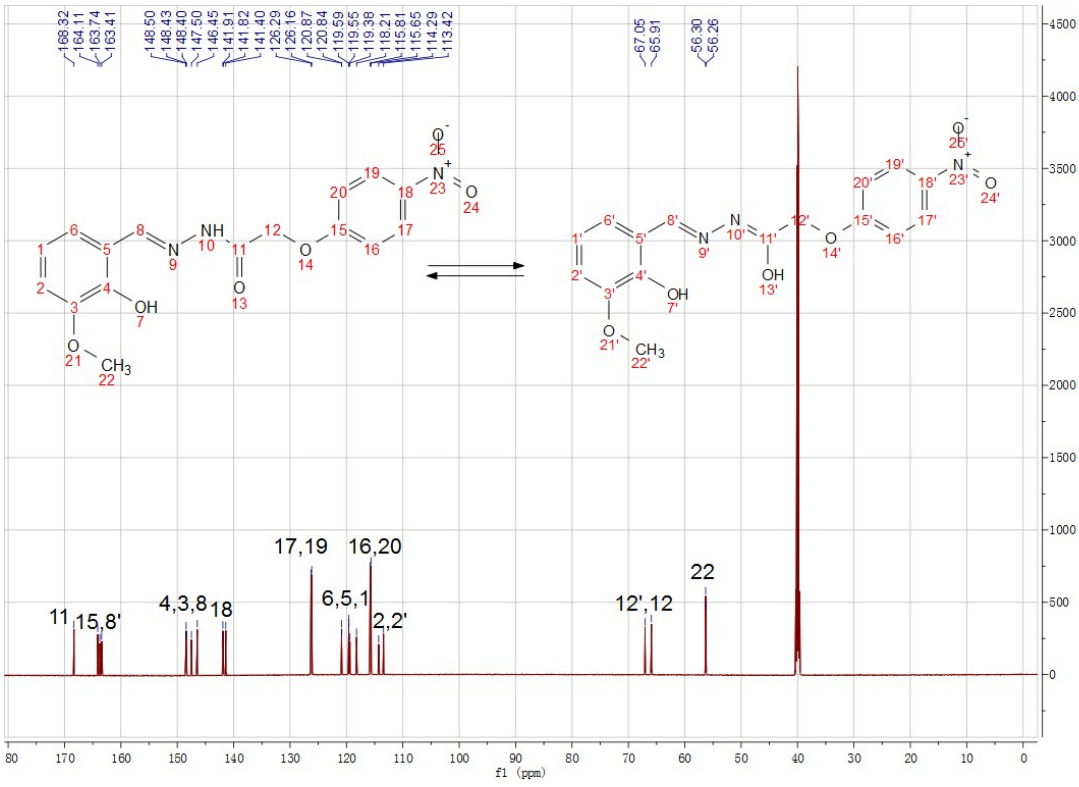

Fig. S6 ^{13}C NMR spectra of the ligand $\mathbf{H_2L^3}$ in DMSO-d^6 solution.

Section 3 Selected Bond Distances (Angles), Distances (Angles) and Hydrogen Bonds for the complexes 1-3

Table S1 Selected bond distances (Å) and angles (°) for **1**[a] , **2**[b] and **3**[c]

		1	
Zn(1)-O(4)	2.003(7)	O(2)#1-Zn(1)-O(2)	79.8(3)
Zn(1)-O(2)#1	2.015(6)	N(2)-Zn(1)-O(2)	84.8(3)
Zn(1)-N(2)	2.053(7)	O(4)-Zn(1)-O(1)	103.5(3)
Zn(1)-O(2)	2.085(7)	O(2)#1-Zn(1)-O(1)	101.9(3)
Zn(1)-O(1)	2.095(7)	N(2)-Zn(1)-O(1)	77.0(3)
Zn(1)-Zn(1)#1	3.146(2)	O(2)-Zn(1)-O(1)	155.1(3)
O(2)-Zn(1)#1	2.015(6)	O(4)-Zn(1)-Zn(1)#1	100.3(2)
O(4)-Zn(1)-O(2)#1	94.5(3)	O(2)#1-Zn(1)-Zn(1)#1	40.69(18)
O(4)-Zn(1)-N(2)	128.8(3)	N(2)-Zn(1)-Zn(1)#1	113.6(2)
O(2)#1-Zn(1)-N(2)	136.1(3)	O(2)-Zn(1)-Zn(1)#1	39.06(17)
O(4)-Zn(1)-O(2)	101.1(3)	O(1)-Zn(1)-Zn(1)#1	137.1(2)
		2	
Zn(1)-O(7)	1.9659(19)	O(5)-Zn(1)-O(3)	93.63(7)
Zn(1)-O(5)	1.9675(18)	O(2)-Zn(1)-O(3)	159.10(7)
Zn(1)-O(2)	2.0094(18)	O(7)-Zn(1)-N(1)	119.51(8)
Zn(1)-O(3)	2.0888(18)	O(5)-Zn(1)-N(1)	126.48(8)
Zn(1)-N(1)	2.106(2)	O(2)-Zn(1)-N(1)	83.42(8)
Zn(2)-O(1)#1	1.9825(18)	O(3)-Zn(1)-N(1)	76.32(8)
Zn(2)-O(6)	2.0084(19)	O(1)#1-Zn(2)-O(6)	103.09(7)
Zn(2)-O(4)	2.0212(17)	O(1)#1-Zn(2)-O(4)	102.47(7)
Zn(2)-O(2)	2.0426(17)	O(6)-Zn(2)-O(4)	109.40(8)
Zn(2)-O(1)	2.080(2)	O(1)#1-Zn(2)-O(2)	152.09(7)
O(1)-Zn(2)#1	1.9825(17)	O(6)-Zn(2)-O(2)	94.23(8)
O(7)-Zn(1)-O(5)	113.90(8)	O(4)-Zn(2)-O(2)	91.95(7)
O(7)-Zn(1)-O(2)	96.41(8)	O(1)#1-Zn(2)-O(1)	74.78(8)
O(5)-Zn(1)-O(2)	94.29(8)	O(6)-Zn(2)-O(1)	121.68(8)
O(7)-Zn(1)-O(3)	97.99(7)	O(4)-Zn(2)-O(1)	128.27(7)
		O(2)-Zn(2)-O(1)	77.52(7)
		3	
N(1)-Zn(1)	2.057(4)	O(4)-Zn(1)-O(19)	88.33(15)
N(2)-Zn(2)	2.026(4)	O(2)-Zn(1)-O(19)	96.54(15)
N(4)-Zn(3)#1	1.993(4)	N(1)-Zn(1)-O(19)	77.09(15)
N(5)-Zn(4)	2.059(4)	O(1)-Zn(1)-O(19)	160.23(14)

O(1)-Zn(3)	1.984(3)	O(4)-Zn(1)-Zn(3)	76.60(11)
O(2)-Zn(1)	2.077(3)	O(2)-Zn(1)-Zn(3)	77.03(10)
O(2)-Zn(1)	1.981(4)	N(1)-Zn(1)-Zn(3)	122.14(12)
O(3)-Zn(3)	1.997(4)	O(1)-Zn(1)-Zn(3)	38.16(9)
O(4)-Zn(1)	1.967(4)	O(19)-Zn(1)-Zn(3)	160.53(10)
O(5)-Zn(3)	2.012(4)	O(10)-Zn(2)-O(18)	104.18(14)
O(10)-Zn(2)	1.988(3)	O(10)-Zn(2)-O(16)	94.99(15)
O(10)-Zn(4)	2.106(3)	O(18)-Zn(2)-O(16)	101.44(17)
O(11)-Zn(2)	2.380(4)	O(10)-Zn(2)-N(2)	149.77(16)
O(15)-Zn(4)	1.970(4)	O(18)-Zn(2)-N(2)	92.66(15)
O(16)-Zn(2)	2.007(4)	O(16)-Zn(2)-N(2)	106.21(17)
O(17)-Zn(4)	1.967(4)	O(10)-Zn(2)-O(11)	74.15(13)
O(18)-Zn(2)	2.007(4)	O(18)-Zn(2)-O(11)	168.91(16)
O(19)-Zn(1)	2.088(4)	O(16)-Zn(2)-O(11)	89.65(16)
O(20)-Zn(4)	2.096(4)	N(2)-Zn(2)-O(11)	84.49(14)
Zn(1)-Zn(3)	3.1463(18)	O(1)-Zn(3)-N(4)#2	141.57(18)
Zn(3)-N(4)#2	1.993(4)	O(1)-Zn(3)-O(3)	104.09(15)
O(4)-Zn(1)-O(2)	108.29(16)	N(4)#2-Zn(3)-O(3)	106.46(18)
O(4)-Zn(1)-N(1)	146.38(16)	O(1)-Zn(3)-O(5)	100.39(16)
O(2)-Zn(1)-N(1)	103.41(15)	N(4)#2-Zn(3)-O(5)	98.61(17)
O(4)-Zn(1)-O(1)	99.71(15)	O(3)-Zn(3)-O(5)	96.74(18)
O(2)-Zn(1)-O(1)	97.98(15)	O(1)-Zn(3)-Zn(1)	40.29(10)
N(1)-Zn(1)-O(1)	86.53(15)	N(4)#2-Zn(3)-Zn(1)	175.40(13)
O(3)-Zn(3)-Zn(1)	74.96(11)	O(15)-Zn(4)-O(20)	101.04(18)
O(3)-Zn(3)-Zn(1)	76.83(11)	N(5)-Zn(4)-O(20)	76.40(16)
O(17)-Zn(4)-O(15)	113.36(19)	O(17)-Zn(4)-O(10)	99.86(16)
O(17)-Zn(4)-N(5)	126.57(19)	O(15)-Zn(4)-O(10)	91.70(15)
O(15)-Zn(4)-N(5)	119.74(18)	N(5)-Zn(4)-O(10)	84.52(15)
O(17)-Zn(4)-O(20)	88.63(18)	O(20)-Zn(4)-O(10)	160.53(14)

[a]Symmetry transformations used to generate equivalent atoms: #1 -x+1,-y+1,-z+2

[b]Symmetry transformations used to generate equivalent atoms: #1 -x+1,-y+2,-z+1

[c]Symmetry transformations used to generate equivalent atoms: #1 x-1/2,-y+3/2,z-1/2 #2 x+1/2,-y+3/2,z+1/2

Table S2 Distances (Å) and Angles (°) of Hydrogen Bonds for **1**, **2** and **3**.

D–H···A	d(H···A)	d(D···A)	∠D—H···A
1			
O3–H3···O4#1	1.871	2.662	161.73
N1–H1···O5#2	1.961	2.741	150.17
C5–H5B···O5	2.589	3.429	150.5
C8–H8AB···O5	2.481	3.232	137.7
C2–H2B···O6	2.473	3.274	151.3
C12–H12B···O7	2.477	3.338	154.1
2			
O8–H8B···O11#3	1.901	2.635	148.5
C24–H24F···O5	2.586	3.451	150
C17–H17H···O4	2.657	3.606	169.7
C15–H15A···O9	3.186	4.132	168.7
C4–H4···O11	2.414	3.324	166.2
3			
C24–H24A···O8	2.474	3.377	164.0
C9–H9B···O18	2.458	3.412	167.4

Symmetry transformations used to generate equivalent atoms: #1: x+1, y-1, z. #2: -x+1, -y, -z+2. #3: -x+1, -y+1, -z+2.

Section 4 Structural information for 1, 2 and 3

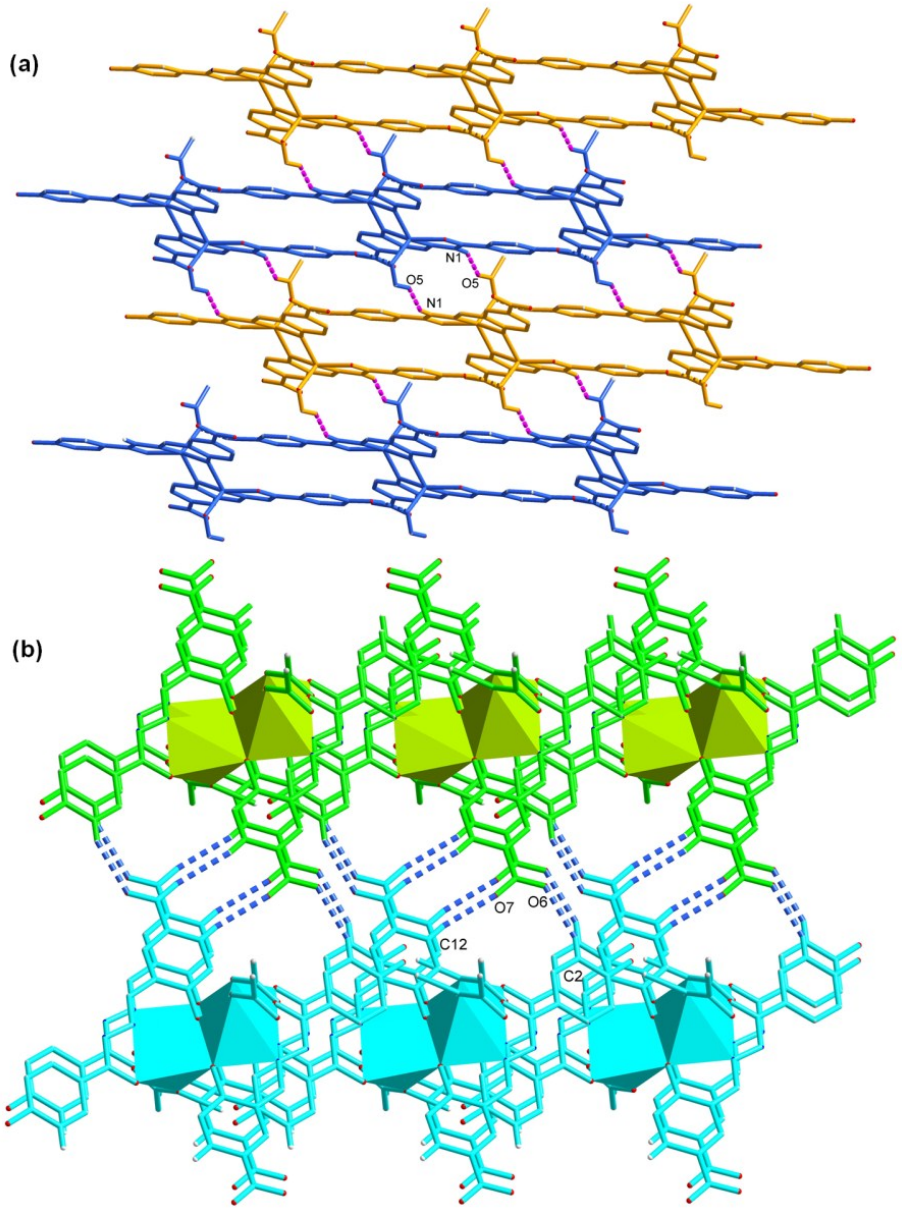

Fig. S7 (a) View of the 2D layer formed by H-bonding interactions of **1** (N1–H1···O5: 1.961, 2.741, 150.17, pink dashed line). Different colors represent different 1D chains. (b) Packing diagram of **1** showing the 3D H-bonded network. Different colors represent different 2D layers (C2–H2B···O6: 2.473, 3.274, 151.3; C12–H12B···O7: 2.477, 3.338, 154.1, blue dashed line).

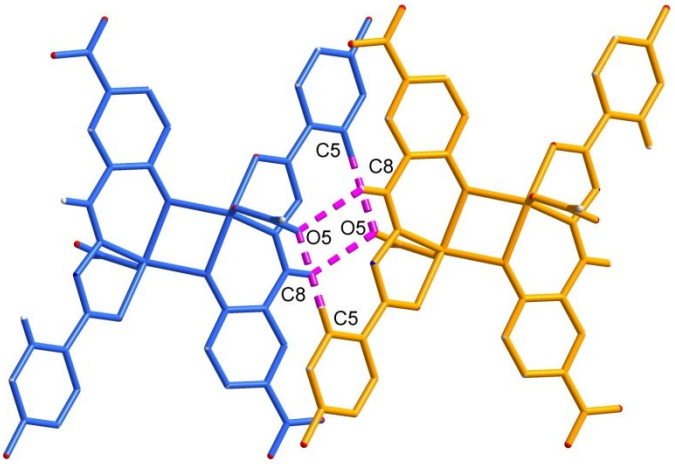

Fig. S8 Hydrogen bonds with C–H···O type in 2D structure of **1** (C5–H5B···O5: 2.589, 3.429, 150.5; C8–H8AB···O5: 2.481, 3.232, 137.7, pink dashed line)

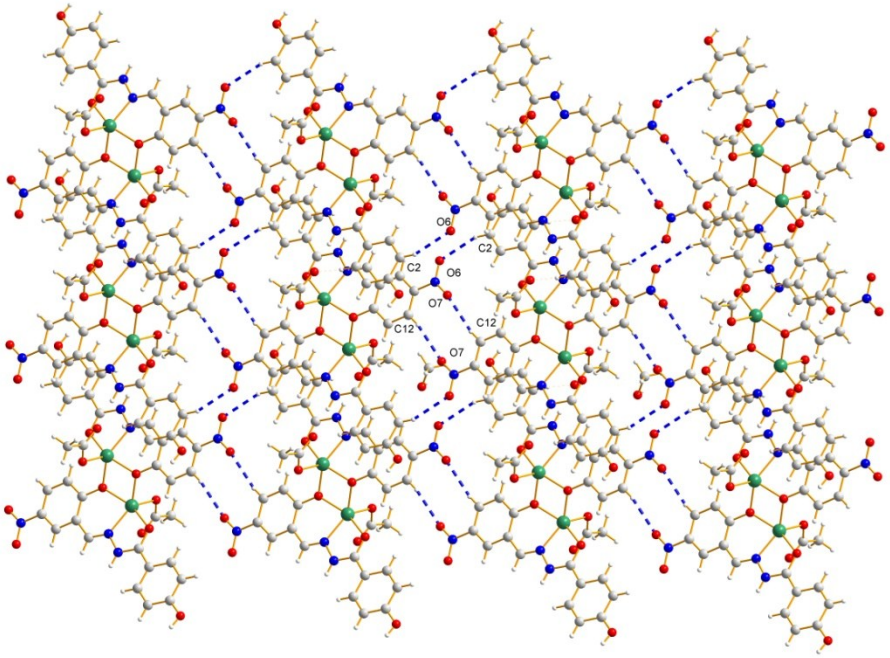

Fig. S9 The 3D packing picture of **1** by H-bonding C2–H2B···O6 and C12–H12B···O7 viewed down from *a* axis (C2–H2B···O6: 2.473, 3.274, 151.3, C12–H12B···O7: 2.477, 3.338, 154.1, blue dashed line).

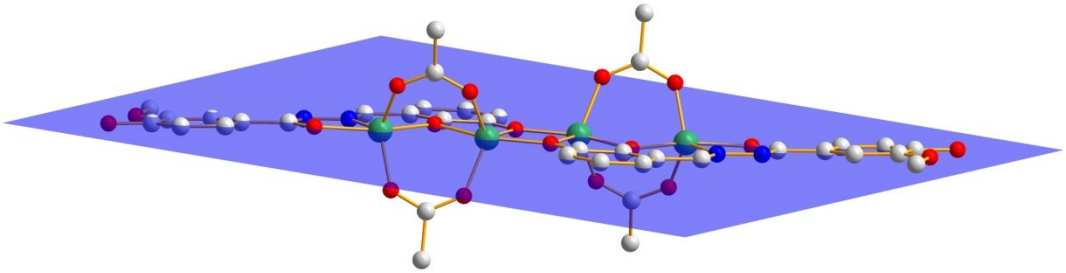

Fig. S10 The coplanar $Zn_4(H_2L_2)_2$ fragment in **2**.

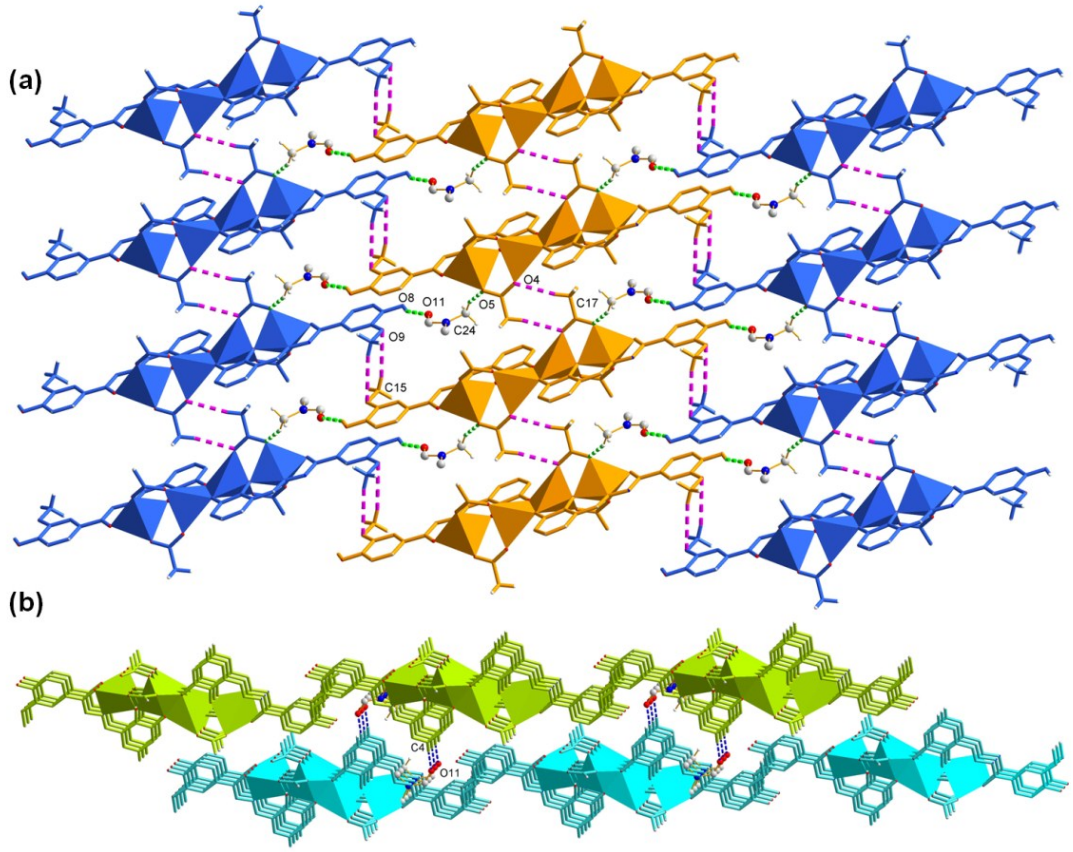

Fig. S11 (a) Packing diagram of **2** showing the 2D H-bonded network (O8–H8B···O11: 1.901, 2.635, 148.5, C24–H24F···O5: 2.586, 3.451, 150, green dashed line; C17–H17H···O4: 2.657, 3.606, 169.7, C15–H15A···O9: 3.186, 4.132, 168.7, pink dashed line). (b) Crystal packing of **2** showing the 3D hydrogen bonding network (C4–H4···O11: 2.414, 3.324, 166.2, blue dashed line). Different colors represent different 2D layers. Hydrogen atoms not involved in H-bonding are omitted for clarity.

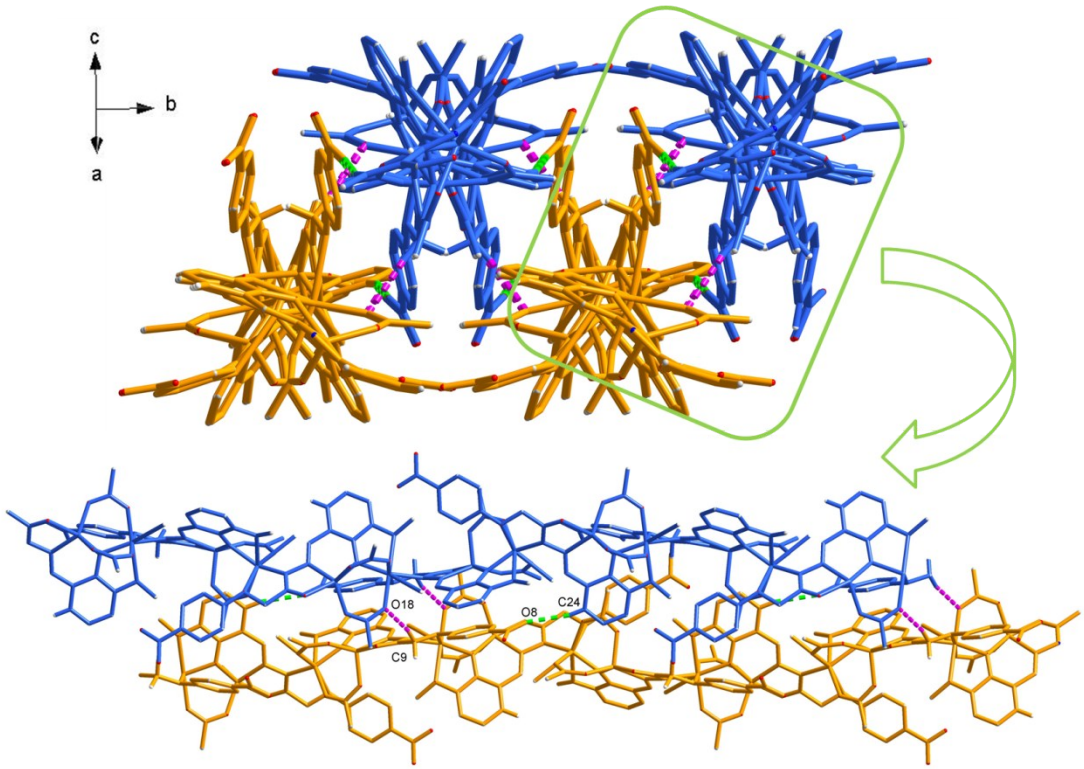

Fig. S12 Packing diagram of **3** showing the 2D H-bonded network (C24-H24A···O8: 2.474, 3.377, green dashed line; 164.0, C9-H9B···O18: 2.458, 3.412, 167.4, pink dashed line). Different colors represent different 1D chains. Hydrogen atoms not involved in H-bonding are omitted for clarity.

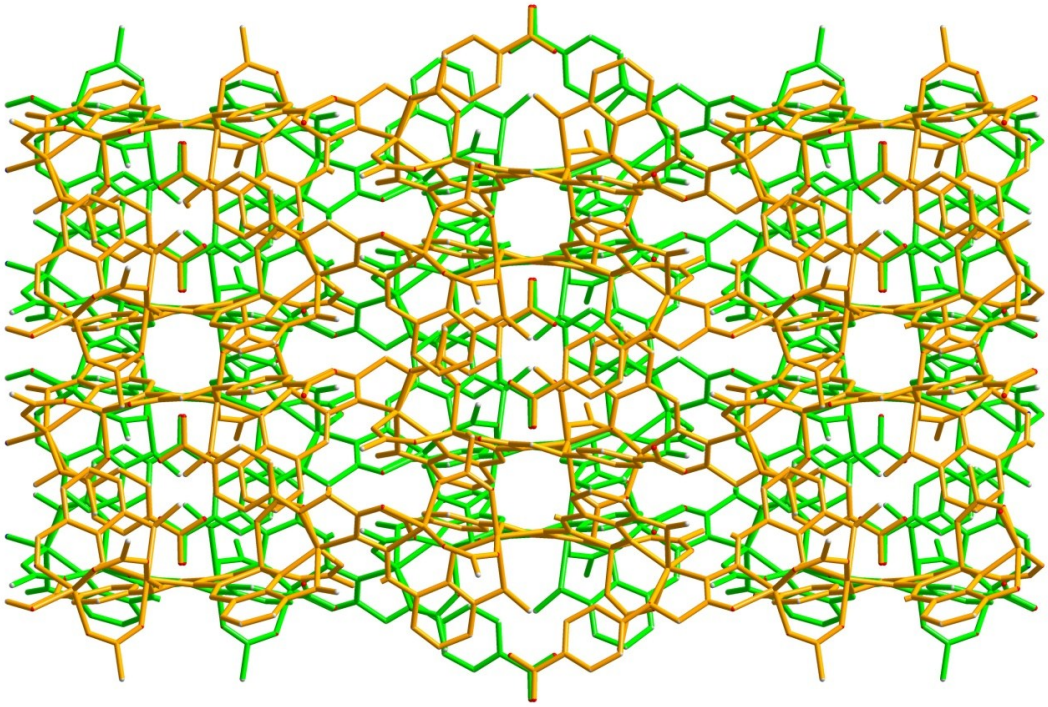

Fig. S13 The 3D packing picture of **3** by Van de Waals interaction. Different colors represent different 2D layers. Hydrogen atoms not involved in H-bonding are omitted for clarity.

Section 5 IR spectrum, PXRD patterns and TGA Curves for 1, 2 and 3.

The simulated and experimental XRPD patterns of three complexes are shown in Fig. S14. All the peaks displayed in the measured patterns match up with those in the simulated patterns generated from single-crystal diffraction data. Their peak positions are in good agreement with each other, indicating the phase purity of the products.

The thermogravimetric analytical (TGA) studies were performed from 25°C to 800 °C at a ramp rate of 10 °C/min in a flowing 50 mL/min nitrogen atmosphere (Fig. S16). In complex **1**, the 3.65% loss should correspond to the loss of one CH_3OH solvent molecule (calculated 3.63%). The TGA curve of **2** displays one distinct stage of weight losses. The stage is from 25 to 230 °C corresponds to the loss of four DMF molecules. The observed weight loss of 20.16% is in agreement with the calculated value of 21.05%. For **3**, the weight loss (6.16%) before 195 °C corresponds to the release of one DMSO solvent molecule (calculated 6.19%).

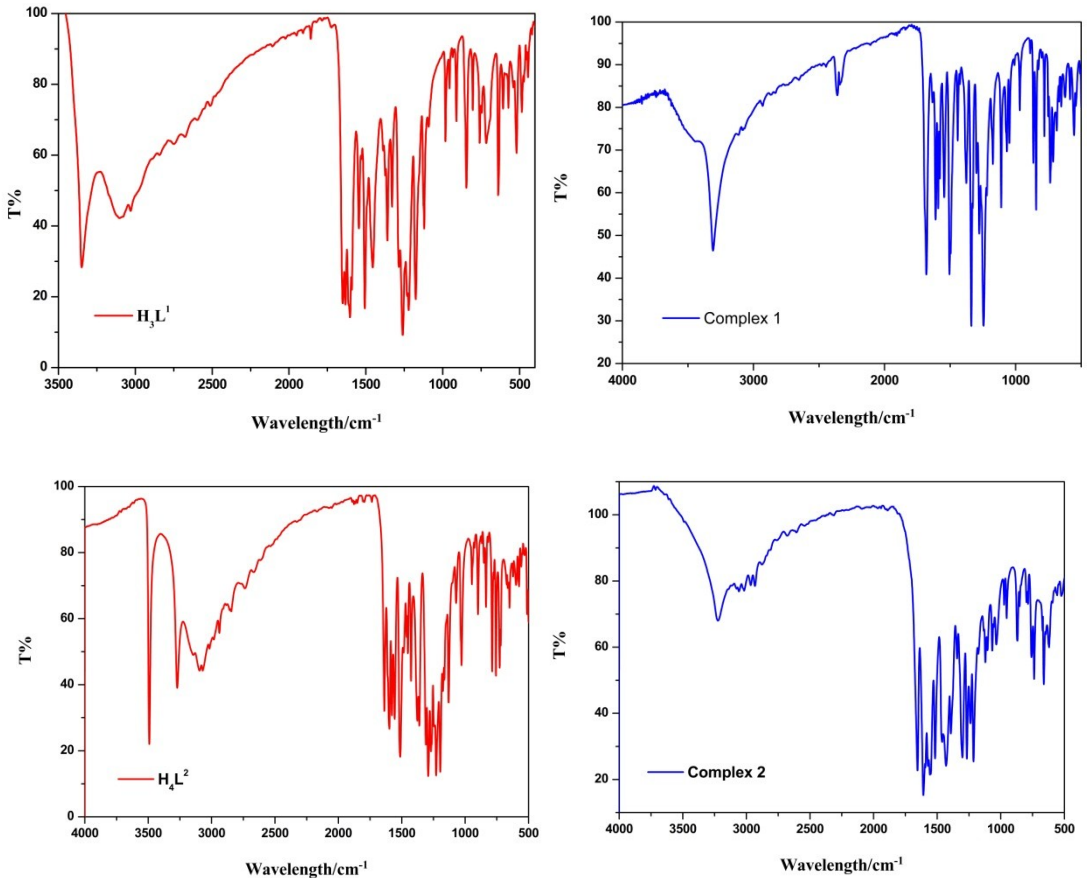

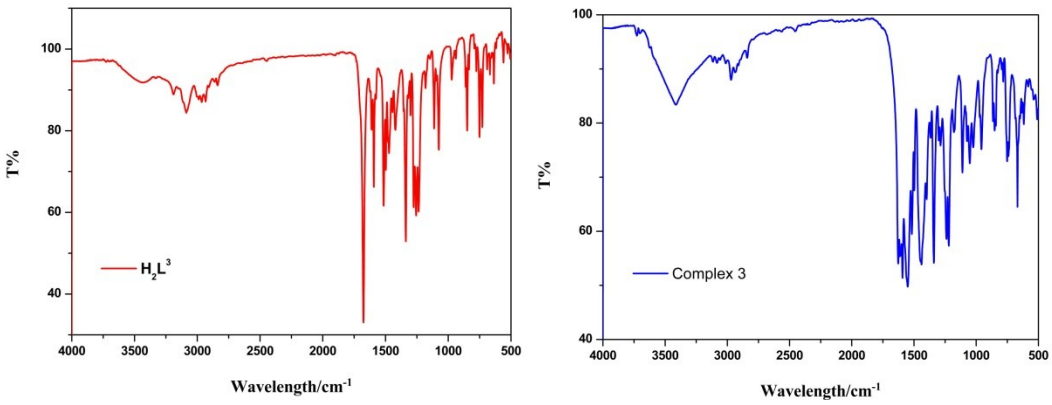

Fig. S14 IR spectra for H_3L^1, H_4L^2, H_2L^3 and complexes **1-3.**

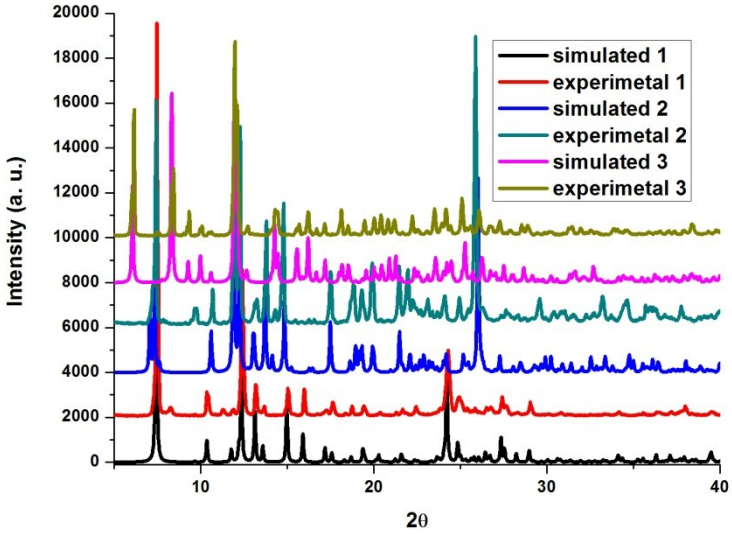

Fig. S15 Simulated and experimental XRPD spectra of complexes **1**, **2** and **3**.

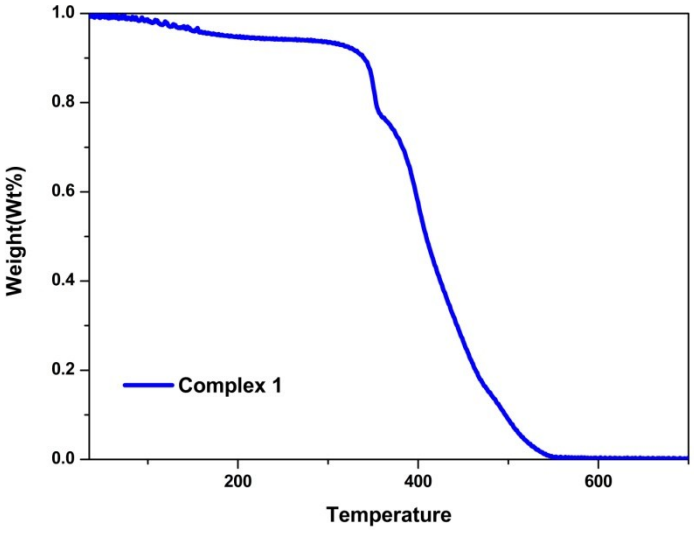

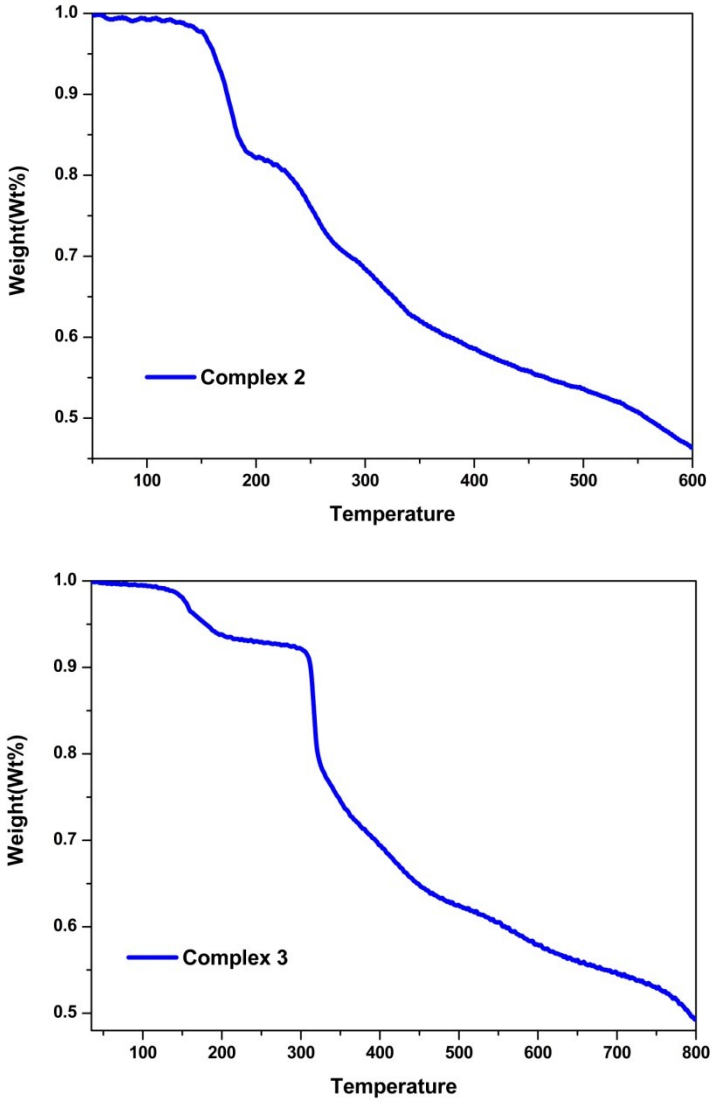

Fig. S16 Thermogravimetric profiles in the temperature range 25-800°C for complexes **1-3**.

Section 6 UV-vis absorption and emission spectra in MeOH

The absorption spectra of complexes **1-3** and free ligands were measured in solid state at room temperature. As shown in Fig. S17, complexes **1-3** exhibit similar spectral profiles to that of ligands ($\mathbf{H_3L^1}$, $\mathbf{H_4L^2}$, $\mathbf{H_2L^3}$), respectively. Three peaks at 313, 384 and 400 nm for **1** are observed, while the $\mathbf{H_3L^1}$ ligand in the $BaSO_4$ plate is observed to absorb at 293 and 394 nm. The high-energy absorption band of ligand $\mathbf{H_3L^1}$ exhibits at 293 nm, which become red-shifted to 313 nm. Meanwhile, absorption band at 394nm of ligand $\mathbf{H_3L^1}$, which splited into two peaks at 384 and 400 nm, upon formation of **1**. The 242 and 344 nm absorption for **2** may be assigned as the π-π* charge transfer, similar to the 232 and 314 nm peaks of the free ligand $\mathbf{H_4L^2}$, the red

shifts for complex **2** compared to the free ligand can be tentatively ascribed to the coordination to metal ions, and the relatively lower peak (~404 nm) is a result of MLCT transition.[1] Two absorption bands at 236 and 309 nm due to the π-π* transitions of the free ligand $\mathbf{H_2L^3}$ (240 and 304 nm) are observed for complex **3**, and the relatively lower peak (~360 nm) is also a result of MLCT transition.

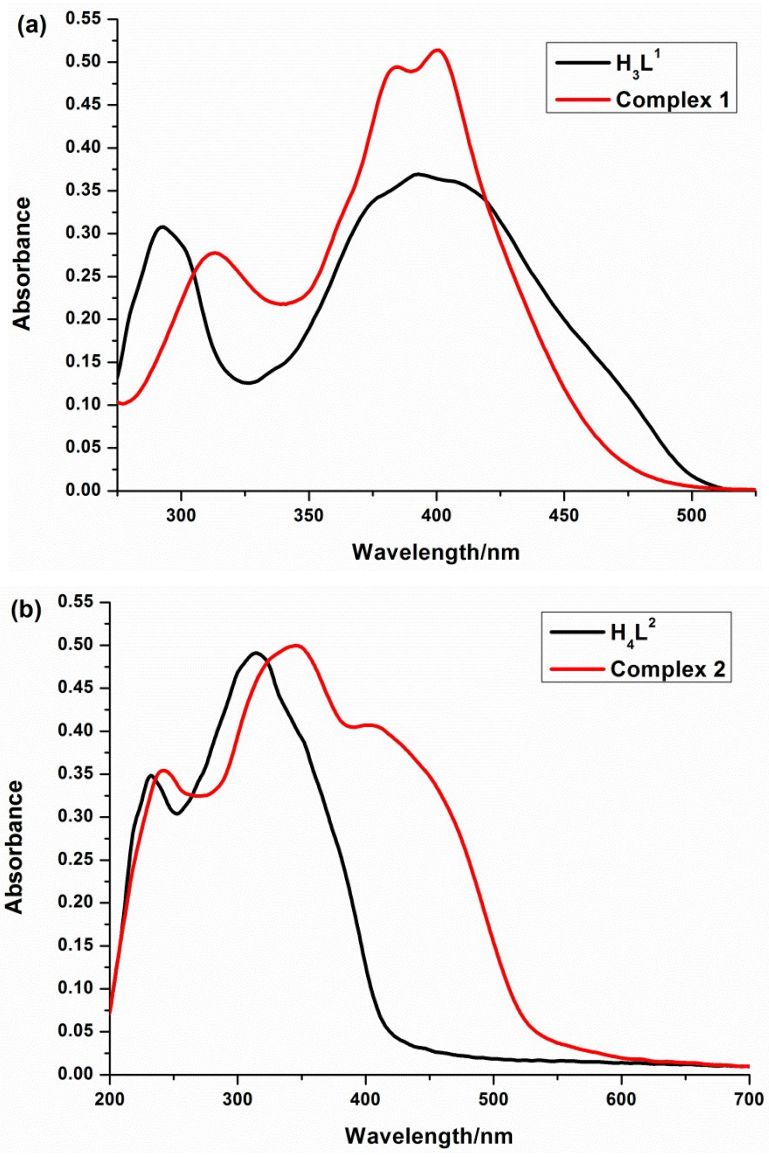

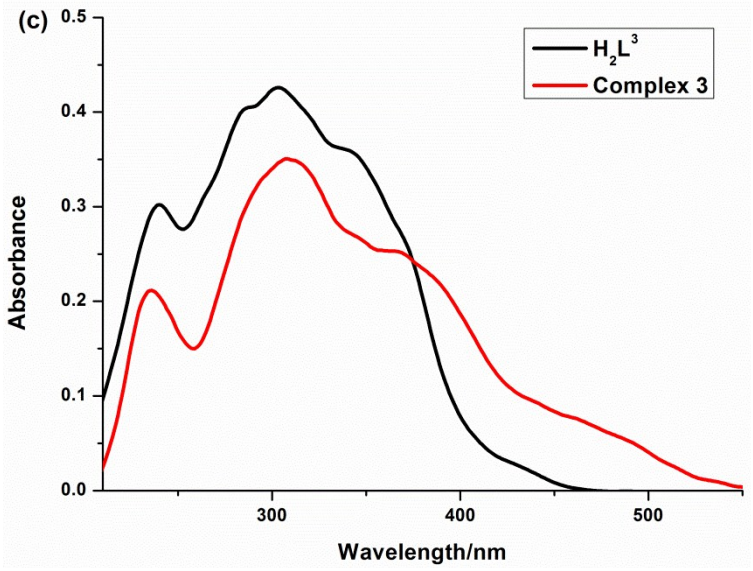

Fig. S17 UV-vis spectra of the $\mathbf{H_3L^1}$ and **1** (a), $\mathbf{H_4L^2}$ and **2** (b), $\mathbf{H_2L^3}$ and **3** (c) in the solid state at room temperature.

The absorption spectra of complexes **1-3** and free ligands were also measured in MeOH, as shown in Fig. S18a. The free ligands present important transitions with absorption bands at ~294 nm for $\mathbf{H_3L^1}$, ~313 nm for $\mathbf{H_4L^2}$ and ~291 nm for $\mathbf{H_2L^3}$, respectively. In the complexes **1-3**, these bands exhibited a red-shift and appeared at ~307 nm for **1**, ~334 nm for **2** and ~310 nm for **3**. Meanwhile, a new maximal absorption peak appeared at ~388 nm for **1** and new relatively lower peaks at ~ 400 nm for 2 and ~ 370 nm for **3**. These changes could be attributed to the interaction between the ligand moiety and zinc. The binding of ligands to Zn^{2+} can form a six-membered chelate ring with the Schiff base C=N and Ar–O-, which enlarges the conjugated system, and reduces the energy difference between n and π^* orbital.[1a,2]

The photoluminescence behaviors of the complexes **1-3** and free ligands in MeOH were also studied (Fig. S18b). The maximum fluorescent emission for $\mathbf{H_3L^1}$, **1**, $\mathbf{H_4L^2}$, **2**, $\mathbf{H_2L^3}$ and **3** were observed at 488, 443, 441, 498, 415 and 458 nm respectively, which are based on the intra-ligand energy transition (IL). Compared with the emission spectra of corresponding free ligand, the blue-shift for coordination complex **1** may be due to that the electron withdrawing of the nitro group at the 5-positon of salicylaldehyde ring enhance the electron transition energy when ligand coordinated with Zn(II) ions. On the contrary, the red-shift for **2** and **3** may be due to that the

coordination of Zn(II) ions enhances the ligand's ability to accept electrons and decreases the electron transition energy. As a result, the HOMO–LUMO energy gap of the complexes decreases.[1a,3]

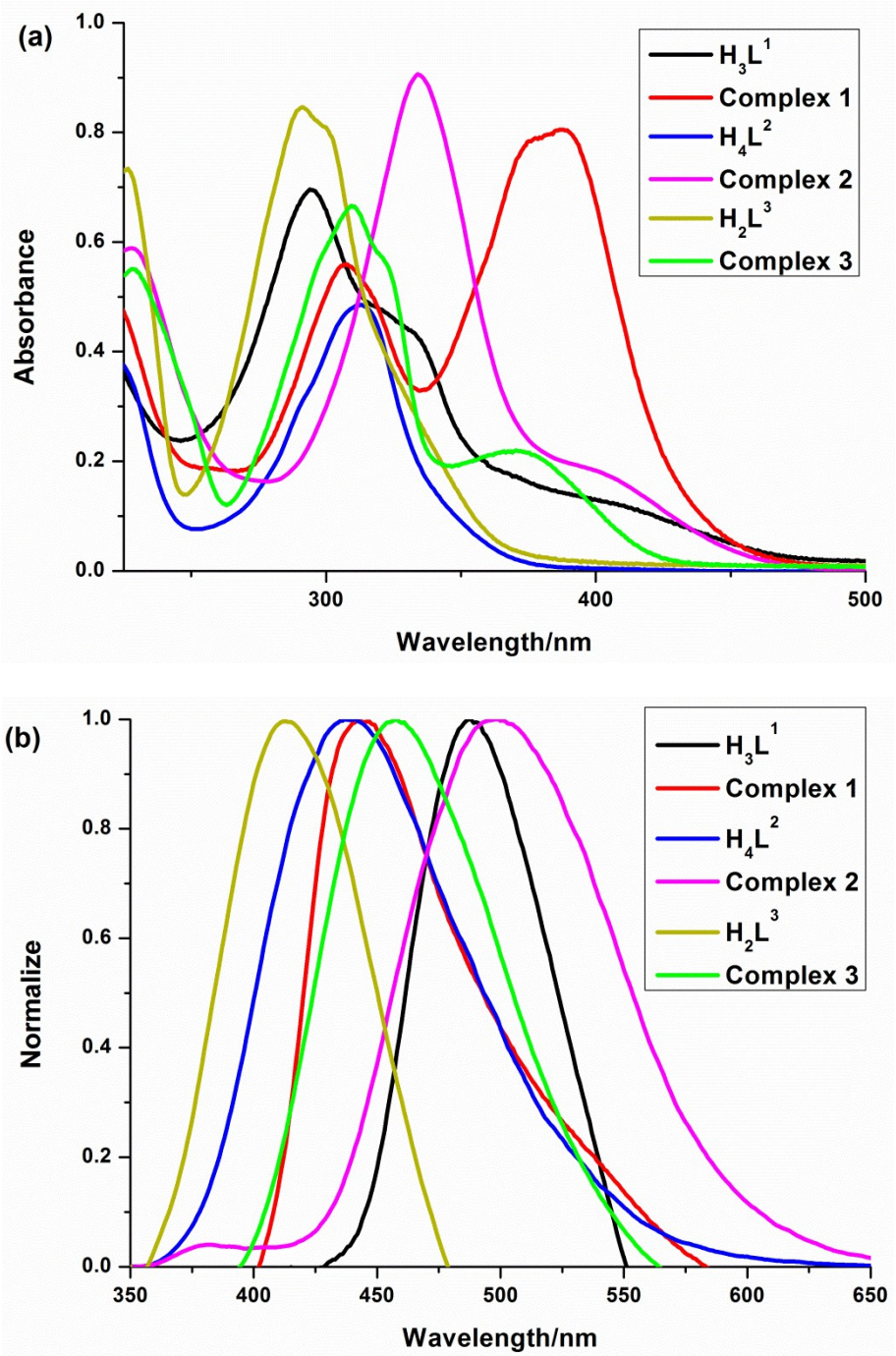

Fig. S18 (a) UV-vis spectra of the H_3L^1, H_4L_2, H_2L^3, **1**, **2** and **3** in MeOH. (b) Normalized emission spectra of the H_3L^1, H_4L^2, H_2L^3, **1**, **2** and **3** in MeOH (30μM in methanol solutions, λ_{ex}= 310 nm).

References

1. (a) B.B. Tang, H. Ma, G. Z. Li, Y. B. Wang, G. Anwar, R. F. Shi, H. Li, *CrystEngComm*, 2013, **15**, 8069–8073. (b) D. Sun, L. L. Zhang, H. F. Lu, S. Y. Feng and D. F. Sun, *Dalton Trans*., 2013, **42**, 3528–3532.
2. X. H. Peng, X. L. Tang, W. W. Qin, W. Dou, Y. L. Guo, J. R. Zheng, W. S. Liu, D. Q. Wang, *Dalton Trans*., 2011, **40**, 5271-5277.
3. (a) V. Chandrasekhar, R. Azhakar, B. Murugesapandian, T. Senapati, P. Bag, M. D. Pandey, S. K. Maurya, D. Goswami, *Inorg. Chem*., 2010, **49**, 4008–4016. (b) J. J. Lu, L. Zhang, L. Liu, G. F. Liu, D. Z. Jia, D. L. Wu, G. C . Xu, *Spectrochim. Acta A*, 2008, **71**, 1036–1041.